Journal of Medicinal Chemistry

Article

Identification of M. tuberculosis thioredoxin reductase inhibitors based on high-throughput docking using constraints

Oliver Koch, Timo Jaeger, Kristin Heller, Purushothama Chary Khandavalli, Jette Pretzel, Katja Becker, Leopold Flohe, and Paul M. Selzer

J. Med. Chem., **Just Accepted Manuscript** • DOI: 10.1021/jm3015734 • Publication Date (Web): 15 May 2013

Identification of *M. tuberculosis* thioredoxin reductase inhibitors based on high-throughput docking using constraints

Oliver Koch[1,2,3], Timo Jäger[2,4], Kristin Heller[2], Purushothama Chary Khandavalli[2], Jette Pretzel[5], Katja Becker[5], Leopold Flohé[2,6], Paul M. Selzer[1,7,8*]*

[1] MSD Animal Health Innovation GmbH, Schwabenheim, Germany

[2] MOLISA GmbH, Magdeburg, Germany

[3]Current address: Technische Universität Dortmund, Chemical Biology, Dortmund, Germany

[4] Helmholtz Zentrum für Infektionsforschung, Braunschweig, Germany

[5] Biochemistry and Molecular Biology, Justus Liebig University Giessen, Germany

[6] Otto-von-Guericke-Universität, Magdeburg, Germany

[7] Universität Tübingen, Interfakultäres Institut für Biochemie, Tübingen, Germany

[8] Wellcome Trust Centre for Molecular Parasitology and Division of Infection & Immunity, University of Glasgow, Glasgow, UK

*Corresponding authors:

Paul M. Selzer

Tel: +49 6130-948-396.

Fax: +49 6130-948-517.

E-mail: paul.selzer@msd.de

MSD Animal Health Innovation GmbH

Oliver Koch

Technische Universität Dortmund

Chemical Biology

Tel.: +49 231 133 2942

E-Mail: oliver.koch@tu-dortmund.de

Keywords: thioredoxin reductase inhibitors, *Mycobacterium tuberculosis*, protein-protein interaction, high-throughput docking,

Abstract

A virtual screening campaign is presented that led to small molecule inhibitors of thioredoxin reductase of *Mycobacterium tuberculosis* (*Mt*TrxR) which target the protein-protein interaction site for the substrate thioredoxin (Trx). *Mt*TrxR is a promising drug target, because it dominates the Trx-dependent hydroperoxide metabolism and the reduction of ribonucleotides, thus facilitating survival and proliferation of *M. tuberculosis*. Moreover, *Mt*TrxR sufficiently differs from its human homologs to suggest the possibility of selective inhibition, if the *Mt*TrxR-Trx interaction site is targeted. To this end, high-throughput docking of 6.5 million virtual compounds to the thioredoxin binding site of *Mt*TrxR combined with constraints as filtering steps was applied. 170 high-scoring compounds yielded 18 compounds that inhibited *Mt*TrxR with IC_{50} values up to the low micromolar range thus revealing that the protein-protein interaction site of *Mt*TrxR is indeed druggable. Most importantly, selectivity towards *Mt*TrxR in comparison to human TrxR (*Hs*TrxR) is also demonstrated.

Introduction

Tuberculosis, thought to be largely defeated during the last century, still accounted for 1.7 million fatalities in 2009 (www.who.int/tb/), the vast majority of which occurred in the developing world. Current first-line treatment is based on only four different drugs, which by now are more than 40 years old. A lack of novel drugs and the mandatory treatment duration of at least 6 months inevitably led to strains with drug and multi-drug resistance. With the development and increasing spread of extensive drug resistance *M. tuberculosis* strains, which often can no longer be treated by any of the available drugs[1,2], tuberculosis is re-emerging as a global threat[3] that demands the search for new drugs with modes of action distinct from those of known ones to minimize the risk of cross-resistance[4].

To this end, the mycobacterial thioredoxin reductase (*Mt*TrxR), here chosen as so far unexploited drug target[5], appeared to offer unique chances but was equally a challenge. In *M. tuberculosis*, *Mt*TrxR reduces the two typical thioredoxins B and C (*Mt*TrxB and *Mt*TrxC) at the expense of NADPH. The functions of the pleiotropic thioredoxins comprise, *inter alia,* i) the peroxiredoxin-mediated reduction of hydroperoxides and peroxynitrite considered to be pivotal for the pathogen's survival in macrophages[6-10]; and ii) likely, as in other species, the synthesis of deoxyribonucleotides indispensable for DNA synthesis and, thus, for proliferation.[11,12] Expectedly, *Mt*TrxR was genetically validated as an essential gene/protein by transposon analysis.[13] Moreover, in other bacteria such as *S. aureus*[14] or *N. gonorrhoeae*[15], TrxR was also shown to be essential for growth. Thus, TrxR inhibitors should compromise multiple pathways in *M. tuberculosis* and, after elucidation of TrxR structures of several species, *Mt*TrxR has become a most promising target for structure-based drug design[16-18].

The primary challenge inherent to this approach is how to inhibit *Mt*TrxR selectively. The human and other mammalian hosts of *M. tuberculosis* contain 3 homologous thioredoxin reductases that fuel similar and equally important metabolic pathways[11] and therefore must not be simultaneously inhibited. Fortunately, all human thioredoxin reductases (*Hs*TrxR1-3) differ from the bacterial ones in one important aspect; their catalytic cycle involves a minimum of 3 redox centres: i) the NADPH binding site with the flavin cofactor, ii) the associated central dithiol-disulfide relay, and iii) a flexible arm with a terminal cysteine-selenocysteine-glycine (CUG) motif[19], which transfers the reduction equivalents from the central dithiol-disulfide relay to the CxxC motif of Trx[20-22]. In contrast, in the low molecular mass TrxRs of bacteria including *Mt*TrxR, the first two redox centres are conserved, whereas the selenocysteine-containing arm is missing and the substrate Trx has to interact directly with the central dithiol-disulfide relay, which in mammalian TrxRs is inaccessible by Trx.[23] Therefore, the TrxR-Trx interaction site in the enzyme of *M. tuberculosis* differs and can be considered unique enough for selective targeting.

However, this encouraging perspective implies another, a technical challenge: the *Mt*Trxs bind to *Mt*TrxR at a protein-protein interaction site which is considered not to be easily druggable. Accordingly, commercial libraries generally show a low hit-rate regarding protein-protein interaction inhibition.[24] In order to increase the chance of detecting low-molecular weight inhibitors, a target-focused library was created using an exhaustive *in-silico* screening campaign that screened a huge chemical space of 6.5 million molecules. The initial screening step here applied, a novel high-throughput docking approach that was complemented with constraints, *a priori* biased the selection towards compounds with high affinity to the Trx binding site of *Mt*TrxR. By means of unbiased re-docking, several filtering steps, scoring, and final consensus

scoring, the huge number of compounds was reduced to 170 candidates for real testing of inhibitory activity. Of those, 18 were proved to inhibit *Mt*TrxR, revealing the efficiency of the *in-silico* screening strategy and the druggability of a protein-protein interaction phase if a large chemical space is explored. Moreover, the inhibitors indeed appear to interact with the Trx binding site typical of the bacterial TrxR, since they do not affect *Hs*TrxR.

Results

Structural comparison of EcTrxR and MtTrxR.

The bacterial TrxR is built up from two domains: an NADPH-binding domain and an FAD-binding domain. There is also ample evidence for substantial conformational change; the NADPH domain rotates approximately 67° during catalysis, which complicates the identification of substrate interaction sites.[23] Most of the available X-ray structures (see experimental section) disclose the F_O conformation (FAD and disulphide side-by-side for flavin ***O***xidation; Figure 1 a and b), in which typically the central redox centre is present as a buried disulphide between Cys135 and Cys138 to be reduced by the $FADH_2$ cofactor. Pdb 1f6m is the only X-ray structure that shows the F_R conformation (FAD and NADPH side-by-side for flavin ***R***eduction; Figure 1 c and d). [25] Here the active site cysteines are reduced and surface-exposed for the reduction of Trx, while the oxidized flavin is in an optimum position for reduction by NADPH.[25] Moreover, this structure represents a dead-end intermediate of the catalytic cycle, revealing the binding mode of Trx to a mutated *Ec*TrxR (*Ec*TrxRC135S). In this mutant, TrxR Cys 138 can still react with the exposed cysteine of Trx (Cys32), but the downstream catalysis via thiol disulphide exchange is no longer feasible, and Trx is arrested in its typical binding mode.

The most prominent interactions are seen between a Trx loop (Tyr70-Ile75) and a complementary cleft on the *Ec*TrxR surface, between Phe141 and Phe142 of the TrxR and a hydrophobic pocket on *Ec*Trx, a hydrogen bond between the Arg73 side chain of Trx and the TrxR backbone carbonyl group of Ala237, and a hydrogen bond between the Asp139 side chain of *Ec*TrxR and the backbone amide of the Trx Ile75 (Figure 2 a and b). The importance of Arg73 in *Ec*Trx has been validated by a loss of activity due to its mutation to Gly and Asp.[26] This presumed Trx binding site is very similar in the F_O and F_R conformation, but in the F_R conformation Trx access is blocked by the rotating FAD domain.

Creating a model for the F_R form of MtTrxR.

The overlay of *Ec*TrxR[25] and *Mt*TrxR[27] reveals high structural similarity in the Trx binding clefts (Figure 2 b/e). In fact, an almost identical binding mode of Trx to TrxR in *M. tuberculosis* can be expected, which is characterized by hydrogen bonding to the corresponding residues Thr242 and Asp149. Therefore, the backbone carbonyl group of Thr242 and the carboxylate of Asp149, separated by a hydrophobic binding cleft (Figure 2e), were chosen as primary target points for putative inhibitors. Unfortunately, this binding cleft and Asp149 are not completely accessible in the only *Mt*TrxR structure available, an F_O conformation in which the FAD domain partially blocks the Trx binding region. However, comparison of the F_R and F_O structures of *Ec*TrxR and *Mt*TrxR reveals that the FAD domain simply rotates away while binding Trx, without otherwise affecting the Trx binding site. This allows creating a model of *Mt*TrxR that mimicked its F_R form by just removing the FAD domain (see Figure 2c and d). Additional flexibility was introduced by allowing different conformers for Asp149 during docking, since Asp 149 can adapt for optimal hydrogen bonding during ligand binding.

From a virtual library to active compounds

The initial high-throughput docking of 6,433,706 compounds of a virtual library of purchasable compounds yielded 151,768 structures that might bind to *Mt*TrxR via the hydrogen bonds suggested to be mandatory by the *Mt*TrxR model outlined above (see Figure 3). All other compounds were either physically unable to fulfil the constraints (e.g. only one H-bond donor), or the existing hydrogen bonds were too weak to pass the constraint filter with a minimum H-bond geometry value of 0.8. This still unrealistically high number of possibly active compounds was then further reduced to less than 10% via unrestrained re-docking with exhaustive settings in order to obtain reliable docking poses and then filtered again using rescoring with the same hydrogen bonding constraints as in the first filter step. Depending on the scoring function, different numbers of virtual hits remained: 7,334 by Goldscore, 9,931 by ASPscore, and 12,684 by Chemscore (Figure 3 b).

The use of a normalization function[28], which was applied on each docking pose, led to a broader and more balanced distribution of the molecular masses of the top-ranking compounds (data not shown) in comparison to the original scoring, because scoring functions alone tend to prefer compounds with high molecular mass, while small molecules are underrepresented. Finally, consensus scoring was applied as another approach which is especially used, in cases where no data is available as to which scoring function performs best. As observed before (www.ccdc.cam.ac.uk/products/life_sciences/gold/case_studies/__optimum_gold/), scoring by Goldscore complies least with the results of Chemscore and ASPscore. Therefore, two different combinations of the available scoring functions were used to rank the compounds based on a consensus scoring by rank.[29,30]

The 200 top-ranked compounds for the different consensus scoring strategies were chosen as candidates for testing. Finally, 170 compounds were selected depending on scoring rank and ease of availability and subjected to a primary screen for inhibition of *Mt*TrxR. Out of these 170 compounds, 18 exhibited inhibition of *Mt*TrxR. Table 1 shows the structures of representative compounds that inhibited *Mt*TrxR by at least 25% at a concentration of 45 µM (Compounds **1-7** obtained from virtual screening each represent a distinct scaffold). As is evident from Table 2, the concentration dependence of *Mt*TrxR inhibition does not always follow expected rules, most likely due to limited inhibitor solubility with increasing concentrations. Accordingly, IC_{50} values could only be roughly extrapolated from inhibition observed at low inhibitor concentrations. However, compound **1** (OK_TrxR_119) with an IC_{50} value of 12.5 µM already reaches a specific activity that appears promising enough for an optimization project of this 4-aminoquinoline scaffold.

The cluster of four compounds that share a 4-(piperidin-1-yl)aniline scaffold (see Table 1: 2,8-10 and Table 3) and is represented by **2** (OK_TrxR_221) was selected for preliminary optimization. Unrestrained re-docking of all these compounds revealed binding to the pre-selected Trx binding site of *Mt*TrxR, taking advantage of hydrogen bonding to Thr242 and Asp149 and a reasonable fit to the hydrophobic pocket in between (see Figure 4). The 4-(piperidin-1-yl)aniline scaffold was therefore used for synthesis of derivatives based on structure-based design and the assumed binding mode. The scaffold by itself (**8**) already showed an IC_{50} of 33.4 µM and two of the derivates (**9** and **10**) reached IC_{50} values of 15.3 and 15.8 µM, respectively (Table 4). The replacement of 4-(piperidin-1-yl)aniline by 4-(piperidin-1-yl)benzylamine in all three compounds (**8-10**) leads to a complete loss of activity (data not shown). This indicates that the aniline substructure containing a hydrogen-bond donor and an

aromatic ring as a hydrophobic group and capable of a π-π stacking interaction is essential which supports the assumed binding mode.

Selectivity of the TrxR inhibitors

The virtual screening was designed to exploit the differences in Trx binding between *Mt*TrxR and its human orthologues[23] in order to identify inhibitors that selectively target the mycobacterial enzyme. It was therefore attempted to investigate the identified inhibitors of *Mt*TrxR for inhibitory activity on one of its human congeners, the TrxR1 isolated from human placenta (*'Hs*TrxR') in two different test systems, using either a mutant version of the physiological substrate human Trx1(TrxC73S; '*Hs*Trx') or the artificial acceptor substrate DTNB. As high test compound concentrations were required, the evaluation of selectivity proved to be an experimental challenge irrespective of the test systems. The aromatic nature of all test compounds in some cases precluded reliable measurements at 100 μM with the *Hs*Trx-based test at a wave length of 344 nm. But also the DTNB-based system with its more convenient read out at 412 nm was sometimes disturbed by test compound concentrations near the solubility limit. Apparent 'enzyme activations' (negative inhibition values in Tables 2 and 4) likely reflect little else than time-dependent changes in dispersity of system components which add an increment to the absorbance change. Table 2 and 4 list the results for *Hs*TrxR inhibition, as experimentally obtained with the more reliable DTNB assay, whereby the apparent enzyme activations are rated as 'no inhibition'. With these precautions, it can safely be stated that only three of the *Mt*TrxR inhibitors (**1**, **3** and **9**) marginally interfere with *Hs*TrxR when tested at the maximum possible concentration.

Due to the same limitations, only lower limits for selectivity indices (SI) can be estimated. The values listed in Table 2 and 4 are based on the assumption that, presuming a typical concentration response of a reversible inhibitor, an extrapolated IC_{50} for *Hs*TrxR does not exceed 200 or 300 μM, if a compound inhibits the enzyme by <30 or <10%, respectively, or less at 100 μM. With these premises, all inhibitors here presented can clearly be rated as selective for *Mt*TrxR.

Discussion and Conclusion

The common goal of *in silico* screening campaigns is to reduce a huge number of available compounds (e.g. the ZINC library (http://zinc.docking.org/) contains over 14 million purchasable compounds) to a target-focused subset that can be tested for activity with reasonable efforts.[31] This is commonly achieved by pharmacophore filtering, which preselects the hypothetical candidates for drug-like compounds that might bind to the target molecule.[31] In the present investigation, however, we faced the challenge preselecting compounds from the virtual library that bind to the target *Mt*TrxR in a specific way that minimizes the chance of binding to the homologous human proteins. Moreover, the pre-determined binding site was a protein-protein interaction site which is not considered to be likely druggable. Under these premises, a combination of high-throughput docking and the use of strong constraints deemed superior to conventional pharmacophore searches. While the latter hardly discriminate between weak and strong hydrogen bonding interactions, the docking software GOLD[36] allows to identify strong hydrogen bonding interactions, in particular by choosing a high minimum H-bond geometry weight as a constraint (here 0.8 on a scale between 0 and 1). Thereby, only very strong hydrogen bonding interactions were considered.

Despite the comparatively high computational power required for docking, the novel strategy proved to be technically feasible. The fast settings applied in the initial docking run (see Experimental Section) generated preliminary binding poses within ~13 sec per compound on an AMD Opteron 250 processor with 2.4 GHz, and the computational power of the latest processors should manage this task even faster. Depending on the scoring function applied, the huge number of compounds of the starting database could be reduced to 0.11% and 0.20%, respectively, which already corresponds to numbers that can be subjected to real screening. Thus, the high-throughput docking approach can, in principle, be used as an alternative to pharmacophore filtering. As shown here, the number of candidates can be further reduced by means of consensus scoring and normalization functions to an extent that allows highly economic testing in terms of manpower and costs. Most importantly, a hit rate >10% compares very favourably to those obtained for other protein-protein interfaces.[32]

It can only be speculated which of the individual screening and scoring steps had the highest impact on this extraordinary number of hits, since activity testing was only performed with the final compound selection. Likely, however, the initial high-throughput docking already led to substantial enrichment of active compounds, since the improvement of compound selections by means of scoring and consensus scoring in the downstream part of the *in silico* campaign is a commonly accepted and applied approach.[29] The active compounds identified in this manner were not yet rated as efficacious enough to justify an in-depth characterization of their biological activity. However, with IC_{50} values in the low micromolar range, the more active ones can be considered promising enough to be used for a hit-to-lead optimization project[18] and, interestingly, the promising hits have a comparatively low MW and could be considered as fragments to be further modified. Our results, thus, indicate that the hits target a very important

part of the interaction, a "hot spot". Moreover, the hit validation of the compounds belonging to the scaffold cluster **2** as well as the predicted binding modes (see Figure 4) suggests that this compound class indeed targets the binding cleft where Arg 73 of *Mt*Trx binds[26]. The selectivity for *Mt*TrxR, which is equally for the observed for the remaining inhibitors, justifies the conclusion that the virtual screening strategy was successful in pre-selecting the chemical space for compounds that target the Trx binding cleft which is unique to the bacterial TrxRs.

In short, high-throughput docking using constraints is shown to be a useful alternative for pharmacophore filtering to handle million of compounds in a virtual screening. This approach appears to be particularly helpful if the biomedical goal demands the exploitation of difficult targets such as protein-protein interaction sites. The feasibility of this novel approach is exemplified by an *in silico* campaign yielding the very first inhibitors of *Mt*TrxR that specifically target the protein-protein interaction of thioredoxins with the bacterial subfamily of thioredoxin reductases, here specifically *Mt*TrxR, which is distinct from the Trx interaction site of higher organisms' TrxRs. Simultaneously, a novel route is offered to meet the challenges of re-emerging tuberculosis.

Experimental Section

Target structure of MtTrxR

Creating a target model for the F_R form of *Mt*TrxR was made feasible by comparing X-ray structures of *Ec*TrxR (F_O form: pdb 1tde and 1tdf [33]; F_R form: Pdb 1f6m[25]), *H. pylori* (F_O form : pdb 2q0k and 2q0l[34]) and *Mt*TrxR (F_O form: pdb 2a87[27]). The FAD domain was removed from the F_O X-ray structure of *Mt*TrxR yielding a preliminary Δ1-123, Δ251-335 *Mt*TrxR structural model in which the NADPH domain (Ala124-His250) comprising the selected Trx binding cleft

to be targeted exactly corresponded to pdb 2a87. The model of the truncated *Mt*TrxR was protonated using Protonate 3D from the program MOE[35] and used as target structure representing the F_R form of *Mt*TrxR.

Virtual screening workflow

The *Mt*TrxR model, created as described above, was used for all docking runs. The Trx binding site was defined to include all atoms within 15 Å of one of the aromatic hydrogen atoms (HZ) of Phe153. The side chain of Asp149 was set flexible with six rotamers (see Table 5). Docking was performed by means of the docking software GOLD[36], and Goldscore was used as scoring function.

For the initial high-throughput docking of 6,433,706 structures, a maximum of ten different poses were created with genetic algorithm settings set to automatic and 10% search efficiency. The docking run for a single compound was stopped if three poses were within an RMSD (root mean square deviation) of 1.5 Å (early termination option) or if it was physically impossible to fulfil the constraints (part of the constraint option). A protein H-bond constraint was set for Asp149 (either one or the other oxygen of the side chain) and Thr242 (oxygen of the backbone carbonyl-group). A minimum H-bond geometry value of 0.8 representing good H-bond geometry ("perfect geometry" would be a value of 1) and strong hydrogen bonding was empirically identified. A penalty value (here 50) was added to the final score if a constraint did not fulfil this minimum H-bond geometry. Poses not passing this hydrogen bonding constraint could be easily identified, since this penalty value was added to the docking output. Docking time per compound averaged around 13s.

For the re-docking step, docking settings were changed to computationally more expensive ones. Fifteen docking poses were created using genetic algorithm settings set to automatic and 100% search efficiency. The protein H-bond constraints and the early termination option were not used during re-docking. The rest of the settings were identical to the initial high-throughput docking run. Docking time was ~270 s per compound. In order to identify the poses forming the mandatory hydrogen bonds to Thr242 and Asp139, all poses were re-scored by the scoring functions Goldscore[36], Chemscore[37,38] and ASPscore[39] combined with the protein H-bond constraints already used in the first docking run. During rescoring, the docking poses were minimized to the nearest local minimum of the respective scoring function. In-house python scripts were used to parse the output files for the constraint penalties and to extract the compounds for the next step.

The final ranking for compound selection was based on a normalization and consensus scoring strategy. A normalizing function described by Carta et al.[28] was applied to yield a broader distribution of the molecular weight within the top-ranked compounds. For final consensus scoring, two different combinations of scoring functions were applied. One consensus scoring is based on all three scoring functions (see above), and the other is based on the combination of Chemscore and ASPscore. The final ranking was based on a "rank-by-rank" strategy [29], where the averages of rank numbers were used. After removing duplicates, the 200 top-ranked compounds from both strategies were selected as candidates for testing.

Virtual library of purchasable compounds

The underlying virtual library consists of combined libraries from various commercial vendors (Akos Consulting & Solutions GmbH, Basel, Switzerland; Asinex Ltd., Moscow, Russia;

ChemBridge Corporation, San Diego, CA, USA; Chemical Diversity Labs Inc., San Diego, CA, USA; Enamine Ltd., Kiev, Ukraine; InterBioScreen, Moscow, Russia; LifeChemicals Inc., Burlington, ON, Canada; Maybridge, Cambridge, UK; Otava, Kiev, Ukraine; Specs, Delft, Netherlands; TimTec Corp., Newark, NJ, USA; Vitas-M Laboratory Ltd., Moscow, Russia) and collectively contained 6,433,706 virtual compounds.

Screening of potential inhibitors against* Mt*TrxR

*Mt*TrxR activity was determined essentially as described in Jäger *et al.* (2004)[9]. The inhibitory effect of each compound on *Mt*TrxR was measured in triplicates. Obvious outliers from the triplicates were removed. If the standard deviation of the two remaining inhibition values exceeded 25%, the measurement was repeated.

The activity of *Mt*TrxR was obtained by measuring initial velocities monitoring the NADPH oxidation at 340 nm at 25 °C. 10 µM TrxR was incubated with 10 µM *Mt*TrxB, 5 µM *Mt*TPx, 225 µM NADPH, 0.06 - 45 µM compound, 73 µM *t*-butylhydroperoxide (added after the pre-incubation step) in a total volume of 100 µl 50 mM HEPES pH 7.4, 1 mM EDTA for 10 min at 25 °C and started by adding hydroperoxide. No compound was present in the positive controls. No *Mt*TrxR was present in the negative controls. A Tecan Freedom EVO® liquid handling platform was used for pipetting, NADPH consumption at 340 nm was measured with a TecanGENios Pro microplate reader after adding *t*-butylhydroperoxide. The enzymes *Mt*TrxR, *Mt*TrxB, and *Mt*TPx from *M. tuberculosis* were produced by heterologous expression in *E.coli* as described9. NADPH, HEPES and EDTA were obtained from Carl Roth (Karlsruhe, Germany), *t*-butylhydroperoxide from Sigma-Aldrich (St. Louis, MO).

If not otherwise stated, IC_{50} values were calculated using the four-parameter equation model 205 and the option "unlock" from the XLfit add-in (IDBS, Guildford, United Kingdom) in Excel (Microsoft Corporation, Redmond, WA). All values are mean values from at least three independent assays. If atypical concentration dependence at high inhibitor concentrations was observed, estimates of IC50 values were obtained by graphically extrapolating from inhibition data at low inhibitor concentrations assuming regular concentration responses of reversible inhibitors (Hill-coefficient = 1).

Inhibition studies with* Hs*TrxR

NADPH and 5,5'-dithio-bis-2-nitrobenzoic acid (DTNB) were obtained from Sigma-Aldrich. Human placenta thioredoxin reductase 1 ('*Hs*TrxR') and the recombinant human thioredoxin mutant Cys73→Ser ('*Hs*Trx'), which does not form dimers and is stable in enzymatic assays, were produced as described previously.[40,41]

Both DTNB (5,5'-dithio-bis-2-nitrobenzoic acid; Sigma-Aldrich, St Louis, MO) and Trx (as physiological substrate) reduction assays were used to determine the effects of the selected compounds on *Hs*TrxR activity.[40,41] All assays were conducted in 100 mM potassium phosphate, 2 mM EDTA, pH 7.4 in a total assay volume of 500 µl. *Hs*TrxR (final concentration 2.8 nM) and 200 µM NADPH (Sigma-Aldrich, St Louis, MO) were added to the buffer before the inhibitors (up to 100 µM final concentration) were added and the reaction was started with either DTNB (3 mM) or with *Hs*Trx (20 µM). The change in absorbance was monitored at 412 nm (for DTNB; ε = 13,600 M−1cm−1) or at 340 nM (for the NADPH-dependent hTrx assay; ε = 6.22 M−1cm−1) using a HITACHI U-2001 spectrophotometer. All enzyme activity assays and kinetic studies

were carried out in at least three independent experiments at 25 C. Control assays (100% activity) were conducted in the absence of inhibitors.

Purchased compounds

Commercially available compounds were purchased from following suppliers. **1** was ordered as 4-[(6-methoxy-2-methylquinolin-4-yl)amino]phenol from InterBioscreen, Moscow, Russia. **2** was ordered as N-[4-(4-{[2-(methylthio)ethyl]amino}-1-piperidinyl)phenyl]-5-phenylpentanamide from ChemBridge Corporation, San Diego, CA, USA. **3** was ordered as 3-(1H-indol-2-yl)-N-(1H-indol-3-ylmethyl)alanine from Vitas-M Laboratory Ltd., Moscow, Russia. **4** was ordered as N'-{(E)-[2-hydroxy-3-(prop-2-en-1-yl)phenyl]methylidene}-3-(3-methyl-5-oxo-4,5-dihydro-1H-pyrazol-4-yl)propane-hydrazide from Otava, Kiev, Ukraine. **5** was ordered as N-phenyl-3-{1-[(3-phenyl-1H-pyrazol-4-yl)methyl]-4-piperidinyl}propanamide from ChemBridge Corporation, San Diego, CA, USA. **6** was ordered as 3-(2-amino-1,3-thiazol-4-yl)-7-hydroxy-2H-chromen-2-one from InterBioscreen, Moscow, Russia. **7** was ordered as 4-[5-amino-3-oxo-4-(4-phenyl-1,3-thiazol-2-yl)-2,3-dihydro-1H-pyrrol-1-l]benzenesulfonamide from InterBioscreen, Moscow, Russia. **8** was ordered as N-[4-(4-{[2-(3-pyridinyloxy)ethyl]amino}-1-piperidinyl)phenyl]-2-pyrazinecarboxamide from ChemBridge Corporation, San Diego, CA, USA. **9** was ordered as 2-phenoxy-N-[4-(4-{[3-(1H-pyrazol-1-yl)benzyl]amino}-1-piperidinyl)phenyl]acetamide from ChemBridge Corporation, San Diego, CA, USA. **10** was ordered as N-[4-[4-(2-pyridin-3-yloxyethylamino)piperidin-1-yl]phenyl]pyrazine-2-carboxamide from ChemBridge Corporation, San Diego, CA, USA. According to the suppliers' information, the compounds were 92-98% pure.

Chemical synthesis

Solvents and chemical reagents were purchased from chemical suppliers and used without any further purification. Dry solvents were generally purchased in sure seal bottles stored over molecular sieves. Unless otherwise stated, all reactions were carried out under dry nitrogen atmosphere. Progress of the reactions was monitored by thin layer chromatography (TLC) (Merck silica gel $60F_{254}$ plates). After elution, a TLC plate was visualized under UV illumination at 254 nm for UV-active materials. Standard staining reagents were used for visualization. Flash column chromatography was carried out using silica gel finer than 230-400 mesh. ^{1}H NMR spectra were recorded on a Brucker 600 or 400 MHz spectrometer in appropriate solvent using tetramethylsilane (TMS) as internal standard. ^{13}C NMR spectra were recorded on a 150 MHz spectrometer. The chemical shifts are shown in δ ppm.

Qualitative and quantitative purity of the all isolated compounds was established by means of ^{1}H NMR and ^{13}C NMR spectroscopic analysis; also, analytical HPLC/MS (Agilent 1200 Series HPLC equipped with C-18 column, coupled with a Sedex-85, LT-ELSD detector) was used to demonstrate the purity of the compounds. All compounds synthesized were at least 95% pure according to HPLC/MS chromatography.

Preparation of 4-(piperidin-1-yl)aniline **(11)**. EtOH (64 ml) was added to 4-(piperidin-1-yl)nitrobenzene (5.21 g, 25.26 mmol) taken into a 250 ml two-necked, round bottom flask equipped with water condenser and stirred at room temperature to generate a homogeneous solution. Water (44 ml), $Fe_{(s)}$ powder (10.72 g, 191.94 mmol), and finally AcOH (8.60 ml) were

successively added to the reaction. The reaction mixture was heated to reflux under dry nitrogen atmosphere, brought to room temperature after two hours, then diluted with EtOAc (50 ml) and vigorously stirred. The resulting suspension was filtered using a short bed of Celite-R545 over sand. Combined extracts were separated from water. Organic portions were collected and dried over anhydrous $MgSO_4$, filtered, and concentrated. A short flash chromatographic purification on silica gel using CH_2Cl_2/MeOH, (9:1) eluent system, yielded the desired product **11** (4.22 g, 95% isolated yield). The spectral data of the compound compiled reported literature values.

General experimental procedure for the preparation of 4-(Piperidin-1-yl)aniline scaffold compounds. 4-(piperidin-1-yl)aniline (**11**; Figure 5) was added to a 1,2-dichloroethane (DCE) (4 ml/mmol) solution of the aldehyde (1 eq) at room temperature, and finally $Na(OAc)_3BH$ (1.30 eq) was added. The reaction was performed at room temperature under nitrogen atmosphere. After completion, saturated aqueous $NaHCO_3$ was added and the reaction mixture was diluted with EtOAc and vigorously stirred. Layers were separated and the aqueous phase was extracted with EtOAc. Combined organic portions were dried over anhydrous $MgSO_4$, filtered and concentrated in vacuo. Flash chromatographic purification on silica gel using CH_2Cl_2/MeOH, (15:1 to 4:1) eluent system yielded the desired product.

***N-(1,3-benzothiazol-2-ylmethyl)-4-(piperidin-1-yl)aniline* (12).** Following the general experimental protocol **10** was prepared in 50% isolated yield. R_f= 0.24 (CH_2Cl_2/MeOH 15:1); ^{1}H NMR (400 MHz, DMSO-d_6): δ = 1.44- 1.51 (m, 2H), 1.54-1.61 (m, 4H), 2.97-3.04 (dd, *J* = 5.27, 5.69 Hz, 4H), 4.86 (d, *J* =5.69 Hz, 2H), 6.32 (t, *J* = 5.48, 6.54 Hz, 1H), 6.83 (d, *J* = 9.07 Hz, 2H), 7.35-7.42 (m, 3H), 7.48 (dd, *J* = 6.97, 7.42 Hz, 1H), 7.90 (d, *J* = 8.44 Hz, 1H), 8.07 (d, 7.80 Hz,

1H); ^{13}C NMR (150 MHz, DMSO-d_6): δ = 23.92, 24.01, 25.51, 50.37, 61.43, 116.44, 120.34, 120.36, 122.44, 124.89, 126.21, 131.28, 134.35, 148.07, 153.22, 167.86, 175.84. HPLC/MS: $C_{19}H_{21}N_3S$, $[M+H]^+$ requires 324.15; found 324.20.

N-(2-chloro-6-fluorobenzyl)-4-(piperidin-1-yl)aniline **(13).** Following the general experimental protocol **13** was prepared in 55% isolated yield. R_f = 0.56 (CH_2Cl_2/MeOH 9:1); ^{1}H NMR (400 MHz, DMSO-d_6): δ = 1.36 – 1.48 (m, 2H), 1.51 - 1.62 (m, 4H), 2.75 – 2.90 (m, 4H), 4.17 – 4.29 (m, 2H), 5.22 – 5.36 (m, 1H), 6.53 – 6.64 (d, J = 7.40 Hz, 2H), 6.68 – 6.78 (d, J = 7.90 Hz, 2H), 7.16 – 7.22 (m, 1H), 7.27 – 7.37 (m, 3H); ^{13}C NMR (150 MHz, DMSO-d_6): δ = 23.95, 25.84, 52.04, 54.01, 113.17, 114.51, 114.54, 118.73, 118.79, 125.66, 130.06, 130.13, 135.04, 142.36, 143.97, 160.62, 162.26. HPLC/MS: $C_{18}H_{20}ClFN_2$, $[M+H]^+$ requires 319.13; found 319.15.

Ancillary Information

*Corresponding authors:

Paul M. Selzer

Tel: +49 6130-948-396.

Fax: +49 6130-948-517.

E-mail: paul.selzer@msd.de

MSD Animal Health Innovation GmbH

Oliver Koch

Technische Universität Dortmund

Chemical Biology

Tel.: +49 231 133 2942

E-Mail: oliver.koch@tu-dortmund.de

Supporting Information Available: The supporting information contains representative dose response curves for IC_{50} calculation. and virtual screening ranking information. This material is available free of charge via the Internet at http://pubs.acs.org.

Funding sources

The study was supported by the Deutsche Forschungsgemeinschaft (BE1540/11-2) and the Bundesministerium für Bildung und Forschung (0315220A).

Abbreviations used:

DTNB: 5,5'-dithio-bis-2-nitrobenzoic acid

HEPES: 2-(4-(2-Hydroxyethyl)- 1-piperazinyl)-ethansulfonsäure

Hs: Homo sapiens

Mt: Mycobacterium tuberculosis

TPx: Thioredoxin Peroxidase

TrxR: Thioredoxin Reductase

Trx: Thioredoxin

References

1. Aziz, M. A.; Wright, A.; Laszlo, A.; De Muynck, A.; Portaels, F.; Van Deun, A.; Wells, C.; Nunn, P.; Blanc, L.; Raviglione, M. Epidemiology of antituberculosis drug resistance (the Global Project on Anti-tuberculosis Drug Resistance Surveillance): an updated analysis. *Lancet* **2006**, *368*, 2142-2154.

2. WHO. Multidrug and extensively drug-resistant TB (M/XDR-TB): Multidrug and extensively drug-resistant TB (M/XDR-TB): 2010 global report on surveillance and response.WHO/HTM/TB: Geneva, Switzerland, **2010,** 1-71.

3. WHO. XDR-TB - a global threat. *Lancet* **2006**, *368*, 964.

4. Koch, O.; Selzer, P. M. Biologie der Mykobakterien und neue molekulare Targets. *Pharm. Unserer Zeit.* **2012**, *41*, 19-26.

5. Jaeger, T.; Flohé, L. The thiol-based redox networks of pathogens: unexploited targets in the search for new drugs. *Biofactors* **2006**, *27*, 109-120.

6. Bryk, R.; Griffin, P.; Nathan, C. Peroxynitrite reductase activity of bacterial peroxiredoxins. *Nature* **2000**, *407*, 211-215.

7. Hu, Y.; Coates, A. R. Acute and persistent Mycobacterium tuberculosis infections depend on the thiol peroxidase TpX. *PLoS One* **2009**, *4*, e5150.

8. Jaeger, T. Peroxiredoxin systems in mycobacteria. *Subcell. Biochem*. **2007**, 44, 207-217.

9. Jaeger, T.; Budde, H.; Flohé, L.; Menge, U.; Singh, M.; Trujillo, M.; Radi, R. Multiple thioredoxin-mediated routes to detoxify hydroperoxides in Mycobacterium tuberculosis. *Arch. Biochem. Biophys.* **2004**, *423*, 182-191.

10. Master, S. S.; Springer, B.; Sander, P.; Boettger, E. C.; Deretic, V.; Timmins, G. S. Oxidative stress response genes in Mycobacterium tuberculosis: role of ahpC in

resistance to peroxynitrite and stage-specific survival in macrophages. *Microbiology* **2002**, *148*, 3139-3144.

11. Arner, E. S.; Holmgren, A. Physiological functions of thioredoxin and thioredoxin reductase. *Eur. J. Biochem.* **2000**, *267*, 6102-6109.
12. Zahedi Avval, F.; Holmgren, A. Molecular mechanisms of thioredoxin and glutaredoxin as hydrogen donors for mammalian S phase ribonucleotide reductase. *J. Biol. Chem.* **2009**, *284*, 8233-8240.
13. Sassetti, C. M.; Rubin, E. J. Genes required for mycobacterial growth defined by high density mutagenesis. *Mol. Microbiol.* **2003**, *48*, 77-84.
14. Uziel, O.; Borovok, I.; Schreiber, R.; Cohen, G.; Aharonowitz, Y. Transcriptional regulation of the Staphylococcus aureus thioredoxin and thioredoxin reductase genes in response to oxygen and disulfide stress. *J. Bacteriol.* **2004**, *186*, 326-334.
15. Potter, A. J.; Kidd, S. P.; Edwards, J. L.; Falsetta, M. L.; Apicella, M. A.; Jennings, M. P.; McEwan, A. G. Thioredoxin reductase is essential for protection of Neisseria gonorrhoeae against killing by nitric oxide and for bacterial growth during interaction with cervical epithelial cells. *J. Infect. Dis.* **2009**, *199*, 227-235.
16. Marhöfer, R.J.; Oellien, F.; Selzer, P.M. Drug discovery and the use of computational approaches for infectious diseases. *Future Med. Chem.* **2011**, *3*, 1011-1125.
17. Krasky, A.; Rohwer, A.; Marhöfer, R.; Selzer, P.M. Bioinformatics and Chemoinformatics: Key Technologies in the Drug Discovery Process. In *Antiparasitic and Antibacterial Drug Discovery;* Selzer, P., Ed.; Wiley-VCH, Weinhein, Germany, 2009; pp 45-58.

18. Rohwer, A.; Marhöfer, R.J.; Caffrey, C.R.; Selzer, P.M. Drug Discovery approaches toward anti-parasitic agents. In *Apicomplexan Parasites: Molecular Approaches toward Targeted Drug Development*; Becker, K., Ed.; Wiley-VCH, Weinhein, Germany, 2011; pp 3-20.

19. Kryukov, G. V.; Castellano, S.; Novoselov, S. V.; Lobanov, A. V.; Zehtab, O.; Guigo, R.; Gladyshev, V. N. Characterization of mammalian selenoproteomes. *Science* **2003**, *300*, 1439-1443.

20. Gromer, S.; Wissing, J.; Behne, D.; Ashman, K.; Schirmer, R. H.; Flohé, L.; Becker, K. A hypothesis on the catalytic mechanism of the selenoenzyme thioredoxin reductase. *Biochem. J.* **1998**, *332*, 591-592.

21. Birringer, M.; Pilawa, S.; Flohé, L. Trends in selenium biochemistry. *Nat. Prod. Rep.* **2002**, *19*, 693-718.

22. Tatyana, S.; Zhong, L.; Lindqvist, Y.; Holmgren, A., and Schneider, G.. Three-dimensional structure of a mammalian thioredoxin reductase: Implications for mechanism and evolution of a selenocysteine-dependent enzyme. *Proc. Natl. Acad. Sci. U. S. A.* **2001,** *98*, 9533–8.

23. Williams, C. H.; Arscott, L. D.; Müller, S.; Lennon, B. W.; Ludwig, M. L.; Wang, P. F.; Veine, D. M.; Becker, K.; Schirmer, R. H. Thioredoxin reductase two modes of catalysis have evolved. *Eur. J. Biochem.* **2000**, *267*, 6110-6117.

24. Sperandio, O.; Reynès, C.H.; Camproux, A.C.; Villoutreix, B.O. Rationalizing the chemical space of protein-protein interaction inhibitors. *Drug Discovery Today* **2010**, *15*, 220-229.

25. Lennon, B. W.; Williams, C. H., Jr.; Ludwig, M. L. Twists in catalysis: alternating conformations of Escherichia coli thioredoxin reductase. *Science* **2000**, *289*, 1190-1194.

26. Negri, A.; Rodriguez-Larrea, D.; Marco, E.; Jimenez-Ruiz, A.; Sanchez-Ruiz, J. M.; Gago, F. Protein-protein interactions at an enzyme-substrate interface: characterization of transient reaction intermediates throughout a full catalytic cycle of Escherichia coli thioredoxin reductase. *Proteins: Struct., Funct., Bioinf.* **2010**, *78*, 36-51.

27. Akif, M.; Suhre, K.; Verma, C.; Mande, S. C. Conformational flexibility of Mycobacterium tuberculosis thioredoxin reductase: crystal structure and normal-mode analysis. *Acta Crystallogr., Sect. D: Biol. Crystallogr.* **2005**, *61*, 1603-1611.

28. Carta, G.; Knox, A. J.; Lloyd, D. G. Unbiasing scoring functions: a new normalization and rescoring strategy. *J. Chem. Inf. Model.* **2007**, *47*, 1564-1571.

29. Oda, A.; Tsuchida, K.; Takakura, T.; Yamaotsu, N.; Hirono, S. Comparison of consensus scoring strategies for evaluating computational models of protein-ligand complexes. *J. Chem. Inf. Model.* **2006**, *46*, 380-391.

30. Verdonk, M. L.; Berdini, V.; Hartshorn, M. J.; Mooij, W. T.; Murray, C. W.; Taylor, R. D.; Watson, P. Virtual screening using protein-ligand docking: avoiding artificial enrichment. *J. Chem. Inf. Comput. Sci.* **2004**, *44*, 793-806.

31. Klebe, G. Virtual screening: strategies, perspectives and limitations. *Drug Discovery Today* **2006**, *11*, 580-594.

32. Gautier, B.; Miteva, M. A.; Goncalves, V.; Huguenot, F.; Coric, P.; Bouaziz, S.; Seijo, B.; Gaucher, J.-F.; Broutin, I.; Garbay, C.; Lesnard, A.; Rault, S.; Inguimbert, N.; Villoutreix, B.O.; Vidal, M. Targeting the proangiogenic VEGF-VEGFR protein-

protein interface with drug-like compounds by in silico and in vitro screening. *Chem. Biol.* **2011**, *18*, 1631-1639.

33. Waksman, G.; Krishna, T. S.; Williams, C. H., Jr.; Kuriyan, J. Crystal structure of Escherichia coli thioredoxin reductase refined at 2 A resolution. Implications for a large conformational change during catalysis. *J. Mol. Biol.* **1994**, *236*, 800-816.
34. Gustafsson, T. N.; Sandalova, T.; Lu, J.; Holmgren, A.; Schneider, G. High-resolution structures of oxidized and reduced thioredoxin reductase from Helicobacter pylori. *Acta Crystallogr., Sect. D: Biol. Crystallogr.* **2007**, *63*, 833-843.
35. Molecular Operating Environment (MOE), 2011.10; Chemical Computing Group Inc., 1010 Sherbooke St. West, Suite #910, Montreal, QC, Canada, H3A 2R7, 2011.
36. Jones, G.; Willett, P.; Glen, R. C.; Leach, A. R.; Taylor, R. Development and validation of a genetic algorithm for flexible docking. *J. Mol. Biol.* **1997**, *267*, 727-748.
37. Eldridge, M. D.; Murray, C. W.; Auton, T. R.; Paolini, G. V.; Mee, R. P. Empirical scoring functions: I. The development of a fast empirical scoring function to estimate the binding affinity of ligands in receptor complexes. *J. Comput. Aided Mol. Des.* **1997**, *11*, 425-445.
38. Baxter, C. A.; Murray, C. W.; Clark, D. E.; Westhead, D. R.; Eldridge, M. D. Flexible docking using tabu search and an empirical estimate of binding affinity. *Proteins: Struct., Funct., Bioinf.* **1998**, *33*, 367-382.
39. Mooij, W. T.; Verdonk, M. L. General and targeted statistical potentials for protein-ligand interactions. *Proteins: Struct., Funct., Bioinf.* **2005**, *61*, 272-287.

40. Gromer, S.; Arscott, L. D.; Williams, CH. Jr.; Schirmer, R. H.; Becker, K. Human placenta thioredoxinreductase. Isolation of the selenoenzyme, steady state kinetics, and inhibition by therapeutic gold compounds. *J. Biol. Chem.* **1998**, *273*, 20096-20101.

41. Urig, S.; Lieske, J.; Fritz-Wolf, K.; Irmler, A.; Becker, K. Truncated mutants of human thioredoxin reductase 1 do not exhibit glutathione reductase activity. *FEBS Lett.* **2006**, *580*, 3595-3600.

Tables

Table 1: Structures of *Mt*TrxR inhibitors obtained from virtual screening (compounds **1-10**) and preliminary optimization (compounds **11-13**). Numbers in brackets indicate number of compounds with similar scaffold

OK_TrxR_119 (1)

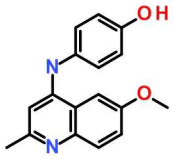

1

OK_TrxR_221 (4)

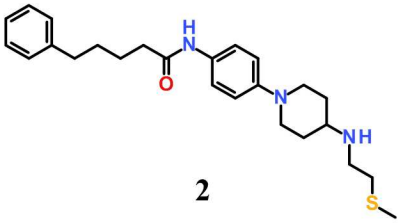

2

OK_TrxR_229 (4)

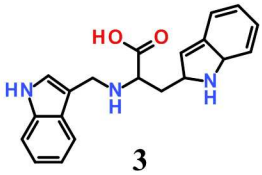

3

OK_TrxR_222 (1)

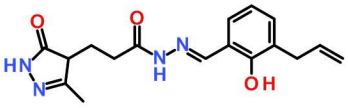

4

OK_TrxR_224 (1)

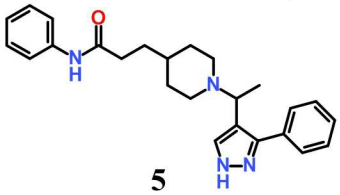

5

OK_TrxR_20 (1)

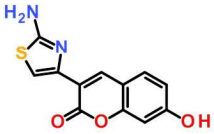

6

OK_TrxR_11 (1)

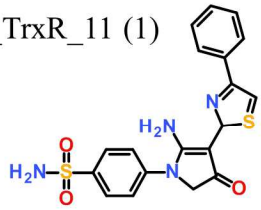

7

OK_TrxR_12

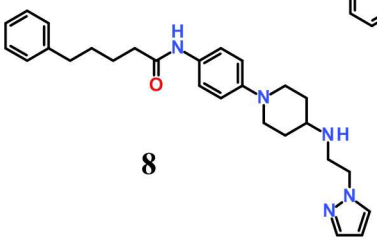

8

OK_TrxR_15

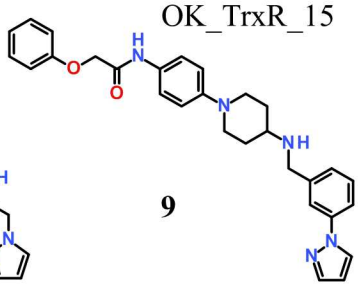

9

OK_TrxR_127

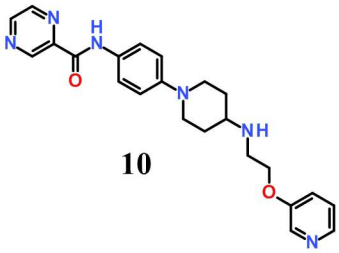

10

OK_TrxR_433

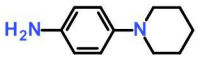

11

CHT240B

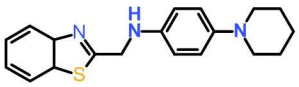

12

CHT236D

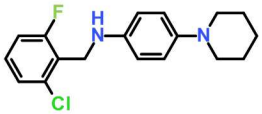

13

Table 2: Inhibition of *Mt*TrxR and *Hs*TrxR by representative compounds obtained from virtual screening in enzyme assays.

Compound no	mean *Mt*TrxR inhibition (%) at				IC_{50} (μM)	mean *Hs*TrxR inhibition (%) at 100 μM[+]	SI***
	45 μM	15μM	5.0 μM	1.67 μM			
1	68.0	51.6	36.0	25.6	12.5	31.6	> 8
2	28.0	33.7	29.7	27.0	~100**	0 (-13.6)	> 3
3	31.0	43.3	31.7	26.7	~ 30**	10.4	> 10
4	26.0	31.7	31.0	31.7	nc[#]	0 (-23.5)	> 10
5	29.8	34.3	38.0	29.7	~ 15**	0 (-2.1)	> 20
6	36.4	19.7	17.3	10.6	~100*	0 (-22.4)	> 3
7	25.0	12.8	9.9	8.4	~200*	0 (-2.6)	> 2

*extrapolated from values below 50% inhibition; **extrapolated from inhibition at low concentrations only; [#] not calculated due to lacking concentration dependence; [+]negative values describe apparent activation likely due to test disturbances at extreme compound concentration; ***estimated selectivity index based on the assumption that 10% inhibition of *Hs*TrxR or less at 100 μM of inhibitor reflects an IC_{50} of >300 μM.

Table 3: Inhibition of *Mt*TrxR of compounds belonging to scaffold cluster of **2**.

Compound no	*mean Mt*TrxR inhibition (%) at			
	45 µM	15µM	5.0 µM	1.67 µM
8	24,0	17,5	14,7	12,3
9	22,1	18,2	16,9	11,2
10	N.A.	16.3	12.0	5.0

Table 4: Inhibition of *Mt*TrxR and *Hs*TrxR by synthesized compounds based on the 4-(piperidin-1-yl)aniline scaffold of **2**.

Compound no	mean *Mt*TrxR inhibition (%) at				IC_{50} (µM)	mean *Hs*TrxR inhibition (%) at 100 µM[+]	SI***
	45 µM	15µM	5.0 µM	1.67 µM			
11	55.0	35.7	17.0	9.5	33.4	0 (-14.4)	> 10
12	67.0	44.4	39.7	24.0	15.8	17.1	> 10
13	58.7	51.7	41.7	30.0	15.3	4.6	> 10

[+]negative values describe apparent activation likely due to test disturbances at extreme compound concentration; ***estimated selectivity index based on the assumption that 10% inhibition of *Hs*TrxR or less at 100 µM of inhibitor reflects an IC_{50} of >300 µM.

Table 5: Asp149 rotamers used for docking

Rotamer	Chi1	Delta1	Chi2	Delta2
1	62	9	-10	19
2	60	8	30	14
3	-177	12	0	30
4	-177	12	65	18
5	-70	10	-15	16
6	-45	10	-111	10

(1-5: GOLD rotamer library, 6: taken from X-ray structure)

Figures

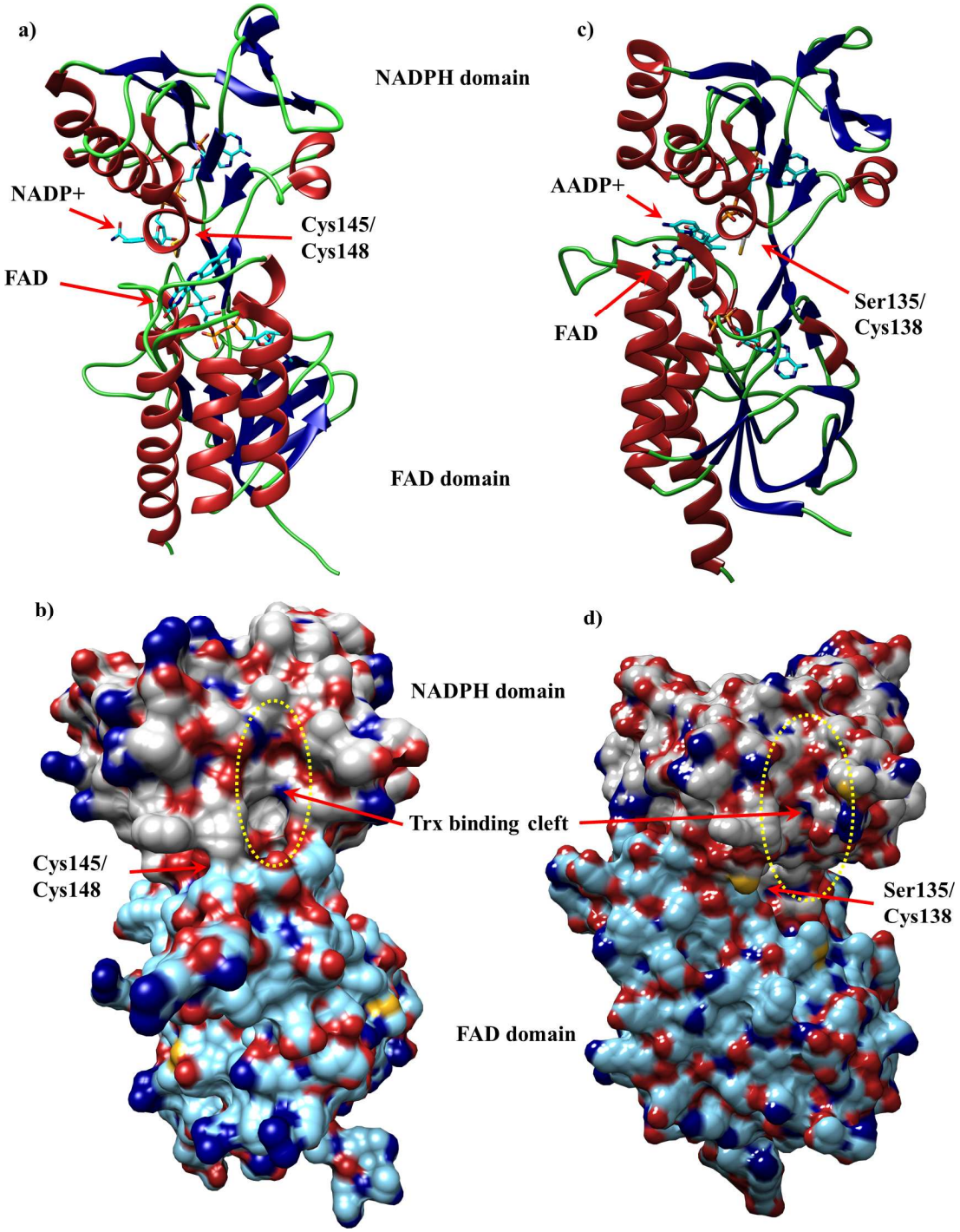

Figure 1

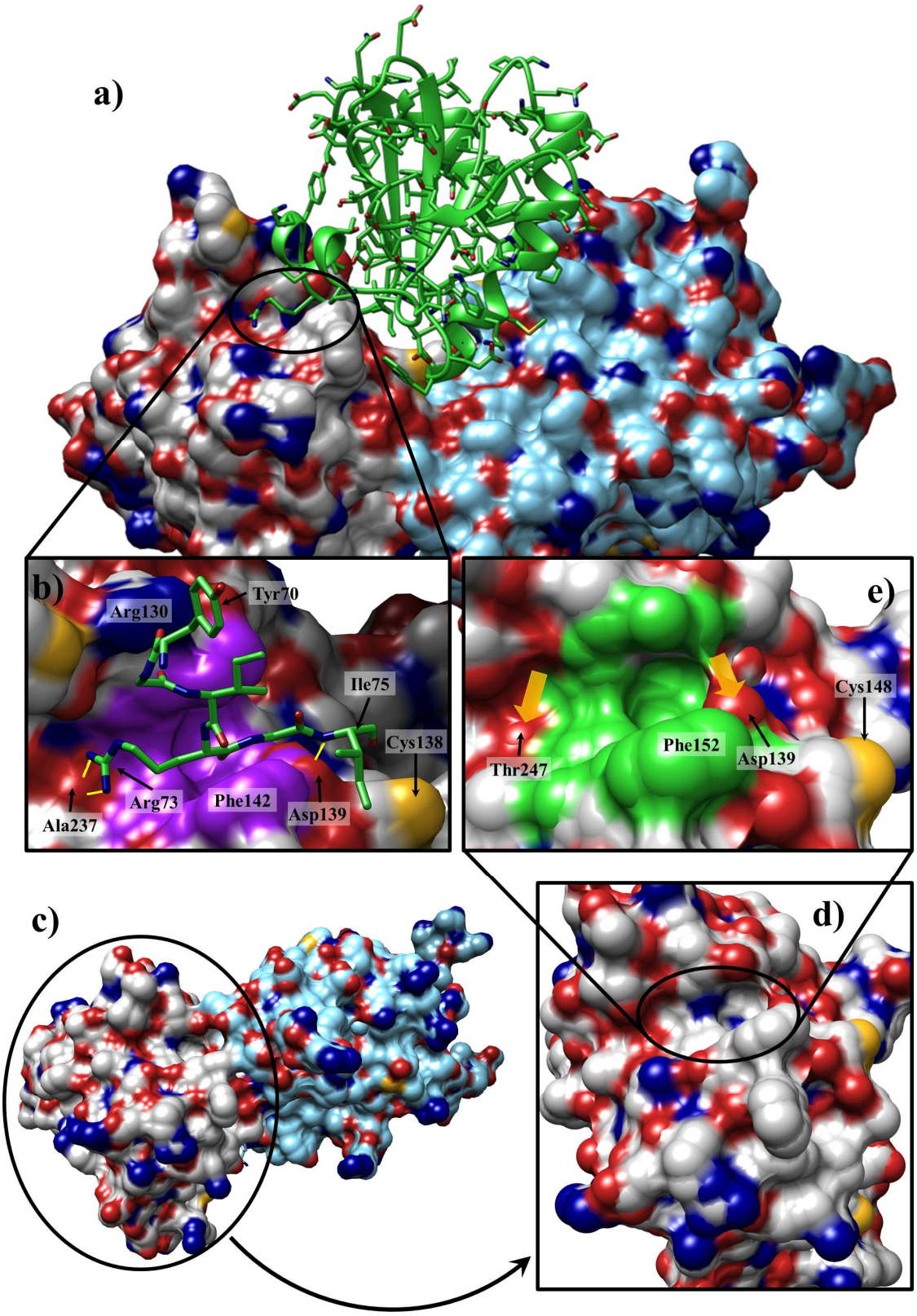
a)
b)
Arg130
Tyr70
Ile75
Cys138
Ala237
Arg73
Phe142
Asp139
e)
Cys148
Phe152
Asp139
Thr247
c)
d)

Figure 2

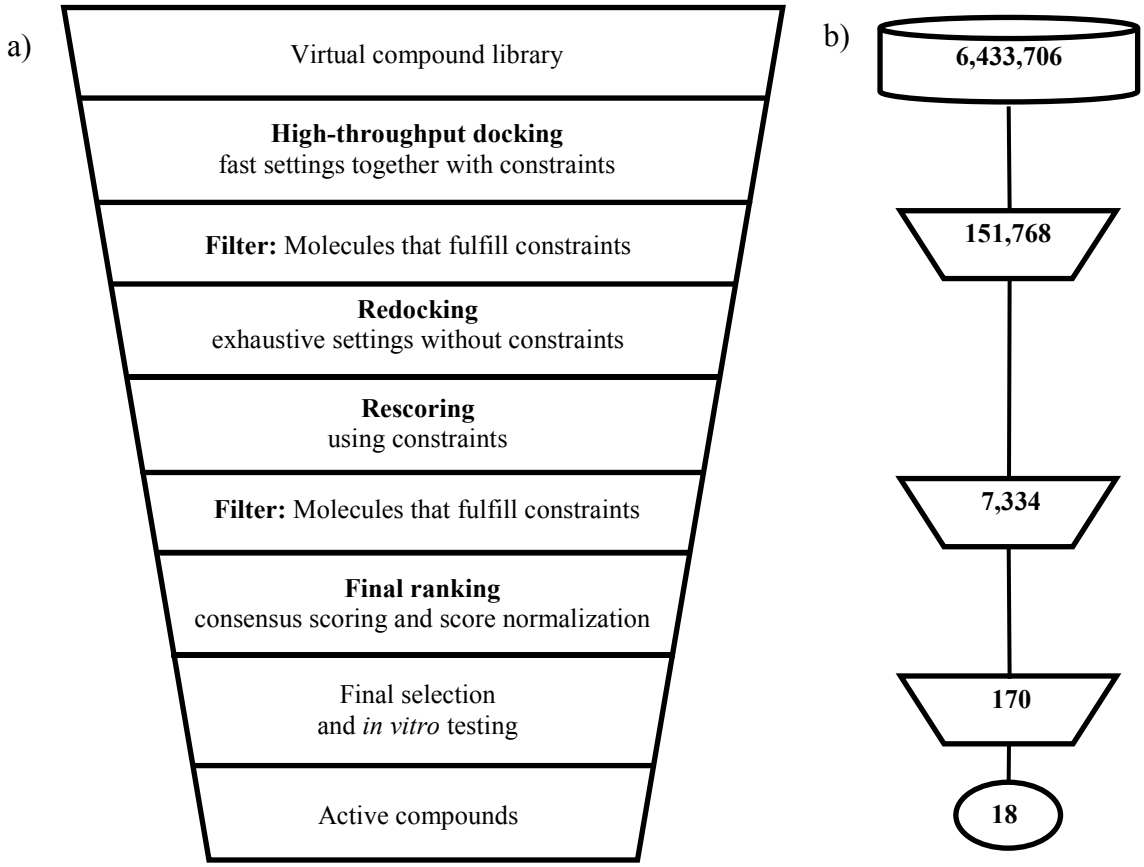

Figure 3

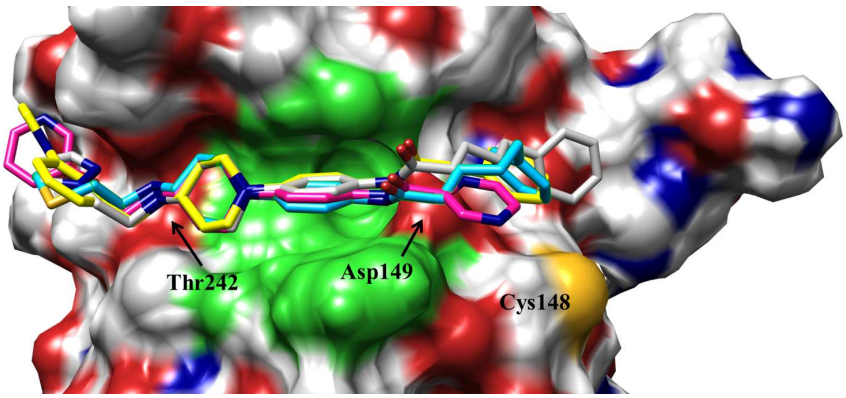

Figure 4

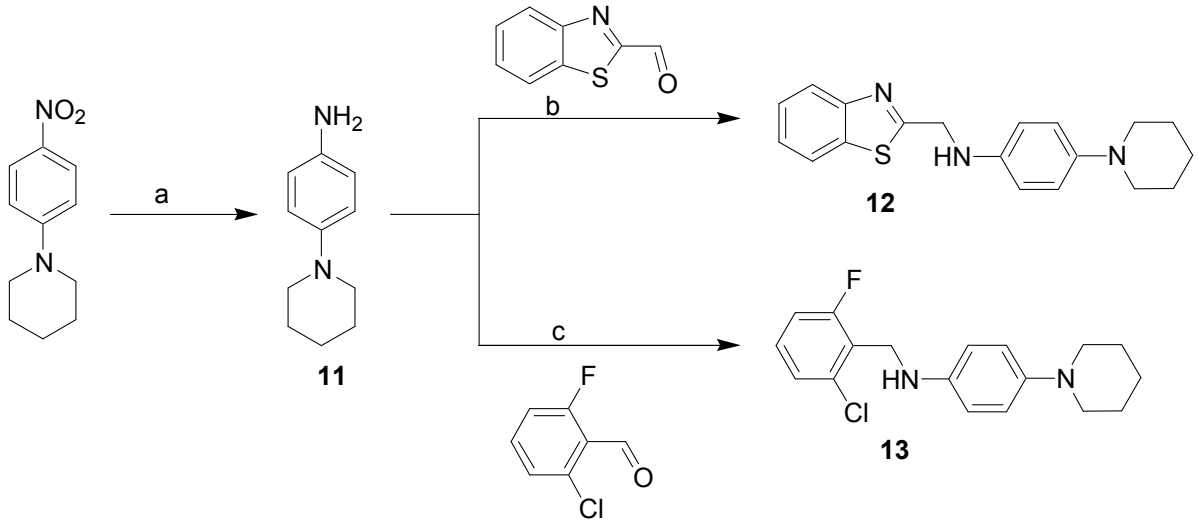

Figure 5

Figure Legends

Figure 1: Comparison of TrxR F_O (a and b, *Mt*TrxR; pdb 2a87[27]) and F_R (c and d, *Ec*TrxR*;* pdb 1f6m[25]) conformations: a) cartoon representation of *Mt*TrxR with $NADP^+$ and FAD bound, and Cys145 and Cys148 marked (red arrows), b) surface representation of *Mt*TrxR (light gray: NADPH domain; light blue: FAD domain, yellow circle: Trx binding cleft) showing the expected Trx binding cleft, c) cartoon representation of *Ec*TrxR with $AADP^+$ and FAD bound, and Ser135 and Cys138 marked (red arrows), d) surface representation of *Ec*TrxR (colours as before) showing the Trx binding cleft.

Figure 2: Essential features of the TrxR-Trx interaction site of bacterial TrxRs. a) X-ray structure (1f6m[25]) showing Trx interacting with *Ec*TrxR (light grey: NADPH domain, light blue: FAD domain, green: Thioredoxin). b) Close-up showing the Trx loop (Tyr70-75) interacting with the binding cleft (magenta surface) and hydrogen bonds (yellow line) to *Ec*TrxR). c) *Mt*TrxR X-ray structure (light grey: NADPH domain, light blue: FAD domain). d) Truncated *Mt*TrxR NADPH domain used during docking. e) Close-up showing the binding cleft (green surface) and the hydrogen acceptors (yellow arrows) addressed during docking.

Figure 3: Virtual screening strategy. a) Generic virtual screening workflow using high-throughput docking and constraints applicable for virtual libraries with millions of compounds. b) Number of compounds that passed the filtering steps from the virtual compound library to active compounds on *Mt*TrxR.

Figure 4: Best docking poses of compounds belonging to the scaffold cluster of **2 (**blue: **2**, grey: **8**, yellow: **9**, magenta: **10)**. The poses are lying within the hydrophobic thioredoxin binding cleft (green surface) near the active site cysteines showing hydrogen bonding interaction with Asp149 and Thr242.

Figure 5: Preparation of 4-(Piperidin-1-yl)aniline scaffolds. (Reagents & Conditions: a. Fe(s)/AcOH, EtOH, reflux, 2 h, 95%.; b. Na(OAc)3BH, DCE, RT, 50%.; c. Na(OAC)3BH, DCE, RT, 55%.),

Table of Contents Graphic